Dissociation dynamics of multiply charged CH_3I in moderately intense laser fields

Arnab Sen,[1] S. Mandal,[1] Sanket Sen,[2] Bhas Bapat,[1] R. Gopal,[3,*] and V. Sharma[2,†]

[1]*Indian Institute of Science Education and Research, Pune 411008, India*

[2]*Indian Institute of Technology Hyderabad, Kandi 502285, India*

[3]*Tata Institute of Fundamental Research, Hyderabad 500046, India*

(Received 20 November 2020; accepted 24 March 2021; published 12 April 2021)

We report on the fragmentation of multiply charged CH_3I ions through dissociative ionization and Coulomb explosion induced by moderately intense (10^{12}–10^{13} W/cm^2) ultrashort laser fields. Velocity map imaging of the fragment ions as a function of pulse duration, ranging from 25 fs to 1.5 ps, leads to kinetic energies, angular distributions, and the relative ion yield in different channels of these fragments. We propose possible pathways for the fragmentation channels based on the kinetic energies and theoretical potential energy curves. For the energetic fragments, we observe an enhanced yield with increasing pulse duration. A simple one-dimensional classical model of wave-packet propagation over the proposed intermediate state potential energy curve is used to estimate the ionization probability as a function of pulse duration. Our results suggest that a delayed enhanced ionization is a consequence of rearrangement of the energies of the molecular orbitals following bond stretching. The resultant energy upshift of the inner orbitals at larger internuclear separation gives rise to resonant multiorbital coupling at a critical distance, which enables enhanced ionization for longer pulses.

DOI: 10.1103/PhysRevA.103.043107

I. INTRODUCTION

The response of molecular systems to intense laser fields of ultrashort (femtoseconds to picoseconds) duration is an intriguing many-body problem which is generally simplified with separation of electronic and nuclear motion on different timescales. Ionization initiated at the peak of the laser pulse is assumed to be instantaneous (few fs), and the consequent nuclear dynamics proceeds in the remnant laser field over longer timescales. However, coupled response of the electronic motion and the nuclear motion lead to several phenomena such as bond softening [1], bond hardening [2], and enhanced ionization [3–5] as observed even in the simplest molecular systems H_2^+/D_2^+. In recent times, many attempts have been taken up to understand intense field interaction with multielectronic molecular systems, based on the understanding of the template molecular systems H_2^+/D_2^+. However, multielectronic molecular systems, such as diatomic molecules, like O_2 [6,7], N_2, HCl, CO, and small polyatomic molecules, like CO_2 [8], NO_2, C_2H_2 [9], CH_3I [10–14], present more complex effects as a consequence of the involvement of multiple electronic states and multiple orbitals, induced by nuclear dynamics. The participation of multiple orbitals even within a single electronic state and the role of the symmetries of these orbitals make for a rich and often inextricable dynamic response of the molecular system.

CH_3I has been a popular molecular system to study ionization, dissociation, and molecular dynamics over many years. CH_3I has a geometry with C_{3v} symmetry, which leads to various distinguishable vibrational motions. The presence of iodine also adds to the complexity with the spin-orbit splitting of the electronic states. Molecular dynamics of CH_3I in the near-infrared (NIR) wavelength regime has only recently been investigated in a few time-resolved studies, incorporating techniques such as transient photoabsorption spectroscopy [15], Coulomb explosion imaging (CEI) of the fragment ions [16,17], and angular streaking of the electrons [18]. These pioneering studies along with a plethora of single-pulse experiments have helped to improve our understanding of the orbitals involved in the nonadiabatic ionization [18,19] and the dominant pathways for dissociation and energetic fragmentation [15,20]. There remain, however, several aspects of molecular ionization and dissociation that have not been addressed yet. In particular, there has been recent interest in understanding the phenomena of enhanced ionization in multielectron molecules. For diatomic molecules, laser-induced electron transfer creates transient ionic states, which are unstable towards ionization. The probability of formation of such ionic states reduces with increasing internuclear separation, and hence the ionization rate is enhanced around a critical range of internuclear distances [21]. An alternative picture considers the effect of geometrically induced alterations in the energies of molecular orbitals at increased internuclear separation, and effective ionization from the laser-coupled orbitals [9,22]. In experiments, the observed kinetic energies in laser-induced fragmentation of CH_3I are usually explained by invoking enhanced ionization beyond the equilibrium bond separation, despite the lack of clarity in the underlying mechanism. At high intensities ($>10^{14}$ W/cm^2) using ultrashort fs laser pulses, the formation of higher charge states is expected, usually triggered by efficient ionization by rescattering electrons. At low to moderate intensities, the route to

*ramgopal@tifrh.res.in

†vsharma@phy.iith.ac.in

the generation of higher charge states is through long ps to ns pulses with wavelengths accessing intermediate resonances in a ladder-climbing mechanism. But with sub ps to ps pulses, the generation of high charge states at moderate laser intensities, as an explicit application of the postulated enhanced mechanisms referred to above, has not been shown.

Here, we report the dynamics of molecular dissociation of multiple charge states of CH_3I following its interaction with moderately intense ($\sim 10^{12}$ W/cm^2) laser fields investigated as a function of varying pulse duration from 25 fs to 1.5 ps. Kinetic energy distributions and angular distributions of the major fragments CH_3^+, I^+, and I^{2+} are ascertained through ion imaging. The analysis of the high-energy fragments systematically shows enhanced ionization with increasing laser pulse duration at a constant laser peak intensity. We use a simple one-dimensional (1D) classical model of wave-packet propagation over the potential energy curve of a proposed intermediate state along with field-free quantum chemistry calculations to model the dynamics of the energy shifts in the orbitals of CH_3I^+. The ionization yield empirically tallies with an enhanced ionization at a critical internuclear distance, at which the energy upshifted HOMO-1 orbital is resonantly coupled with the HOMO orbital in the laser field.

II. EXPERIMENTS

The system delivering the ultrashort laser pulses for our experiment, Femtopower V (Spectra-Physics, Austria), provides few-mJ laser pulses at 1 kHz at a central wavelength of 800 nm, of which a small fraction is used for the molecular physics experiments in the ion-imaging spectrometer [23]. The shortest pulse duration, at the optimum compressor grating pair position, measured just after the laser amplifier unit through autocorrelation, is $\sim$25 fs. Longer pulses can be obtained by varying the separation between the compressor grating pair. The corresponding pulse duration is estimated from the dispersion curve for the grating pair supplied by the manufacturer. A scan of the grating separation and the corresponding second harmonic spectrum obtained through a thin KDP crystal (0.5 mm, Eksma Optics, Lithuania) allows us to characterize the pulse and grating dispersion characteristics [24] and hence refine the estimates. For pulse durations beyond 75 fs, the dispersion characteristics and hence the pulse widths are determined largely by the grating compressor with a residual error of $\sim$10%. The polarization of the laser beam is linear and can be set parallel and perpendicular to the ion-imaging spectrometer axis by using a $\lambda/2$ plate (B-Halle, Germany). The laser beam is focused in the spectrometer chamber by using a thin lens with a focal length of $f = 30$ cm, which focuses the beam to a measured spot size of ~ 70 μm. A peak laser intensity of $I_0 = 5 \times 10^{12}$ W/cm^2 is thereby estimated. The intensity values are calibrated independently in a COLTRIMS set up using the same laser focusing geometry, where, features in the ion spectrum can be used to extract the intensity in the focus [25].

The details of the spectrometer and the extraction of three-dimensional velocity distributions of the laser-induced fragmented ions are discussed in Gopal *et al.* [23]. Vapor from 99.5% CH_3I procured from Sigma-Aldrich is allowed to effuse into the chamber through an orifice close to the laser focus. The spectrometer is used in two different modes: (a) the standard imaging mode, where the laser polarization axis is kept perpendicular to the spectrometer axis to obtain the three-dimensional (3D) velocity distribution of the fragment ions, and in (b) the time-of-flight (ToF) mode with the polarization axis parallel to the spectrometer axis. The laser pulse energy is adjusted to maintain the same peak intensity for the different pulse durations. For each laser pulse duration setting, velocity distributions for the different ions are obtained for the same amount of time (2 h), ensuring the same number of laser shots (within $\pm$5%) and constant gas pressure throughout. The spectrometer voltages for imaging each of the fragments are optimized to ensure velocity images are fully contained within the detector area.

The flight times of the ions in the ToF mode can be used to calculate kinetic energies and thus confirm the ion kinetic energies obtained from the velocity distribution. Furthermore, the multihit capability of the detector (Roentdek GmbH, up to 8 ions with a double hit dead time of $<$10 ns) is also exploited to check if there are any coincident ions recorded in the second hit. Through photoion-photoion coincidences, back-to-back breakup channels, resulting in high-energy ions, can be unambiguously identified, and their mean ion energies ascertained [23]. The gas pressure is kept low enough to have an ion count rate of less than 300 Hz for all ions to avoid false coincidences on the imaging detector and any possible space charge effects. Using the gratings to stretch the laser pulse inevitably introduces wavelength dispersion into the laser pulse. All measurements reported here are done with a positive (dominant) second-order dispersion. The effect of the sign of the dispersion is checked by obtaining spectra for a few pulse duration settings but with negative second-order dispersion and differences are found to be insignificant.

III. RESULTS

Figure 1(a) shows the ToF spectrum of the ionic fragments arising from the interaction of methyl iodide with an 800-nm, 1500-fs laser pulse with peak intensity I_0. The dominant peaks are the parent ion CH_3I^+, the singly charged methyl group $CH_n{}^+$ ($n = 0-3$), and the iodine ions I^{q+} ($q = 1-2$). The photoion-photoion coincidence spectrum shown in Fig. 1(b) identifies ions obtained in pairs from the fragmentation of the same molecular ion. Two prominent sets of islands, which represent the coincident detection of the fragment pairs (a) $CH_n{}^+ + I^+$ and (b) $CH_n{}^+ + I^{2+}$ are highlighted. Each set contains four pairs of islands associated with coincident detection of $CH_3{}^+$, $CH_2{}^+$, CH^+, and C^+ ions with I^+/I^{2+}. However, several uncorrelated events indicated as false counts are also detected on the diagonals between the island pairs. The islands are, however, separated and with suitable conditions imposed the coincident events can be uniquely extracted for analysis. The nature of these islands in the coincidence map indicates a concerted, energetic, back-to-back breakup from the molecular ions CH_3I^{2+} and CH_3I^{3+}, respectively. Keeping the peak laser intensity fixed, spectra are obtained at various pulse durations from 25 to 1500 fs.

Figure 2(a) (top) shows the variation in the obtained yield as derived from the area under the peaks in the ToF spectrum. The yield of the parent molecular ion CH_3I^+ shows an

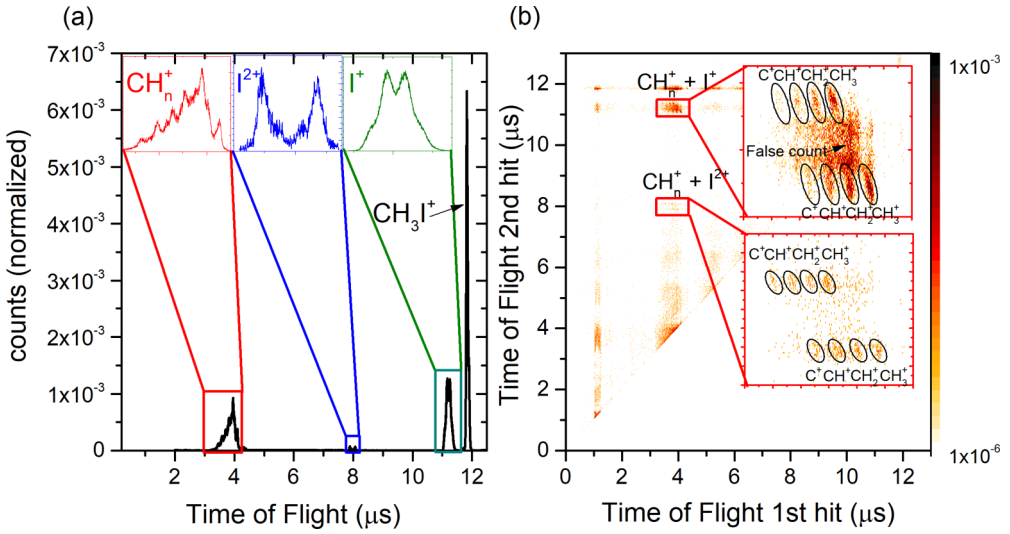

FIG. 1. (a) The ToF spectrum at a pulse duration of ∼1500 fs with peak intensity 5×10^{12} W/cm^2 with the main fragments highlighted and their peaks shown in an expanded form. (b) The corresponding photoion-photoion coincidence map of the first two consecutive hits of the fragments. The color scheme representing ion count density is in the logarithmic scale. Islands corresponding to $CH_n^+ + I^+$ and $CH_n^+ + I^{2+}$ are highlighted and expanded.

insignificant variation with pulse duration as compared to the yield of other ionic fragments. A prominent change is seen for the high-energy fragments in the $CH_n^+ + I^+$ islands, with a monotonic increase in their yields until about 1000 fs and then a saturation [Fig. 2(a) (bottom)].

The method of changing the pulse duration also introduces dispersion in wavelengths within the pulse duration, that is, a chirp in the pulse. It is therefore important to verify that the observations noted above are mainly pulse-width dependent and that the role of chirp may be disregarded. Towards that, in Fig. 2(b) we plot a 2D contour map of the ion yield for the main fragments at various grating position offsets (with respect to the grating position for shortest pulses). Positive offsets introduce a positive chirp of ∼4700 fs^2/mm. The spectrum at each grating position is normalized to total counts obtained for that setting. That the spectra are identical for positive and negative chirps indicates that in this intensity range and particularly for fragmentation products, the role of chirp may not be too significant.

Three-dimensional ion velocity distributions are obtained for CH_3^+ and I^+ fragments for the pulse durations of 25, 150, 250, 650, 950, 1300, and 1500 fs, keeping the same laser

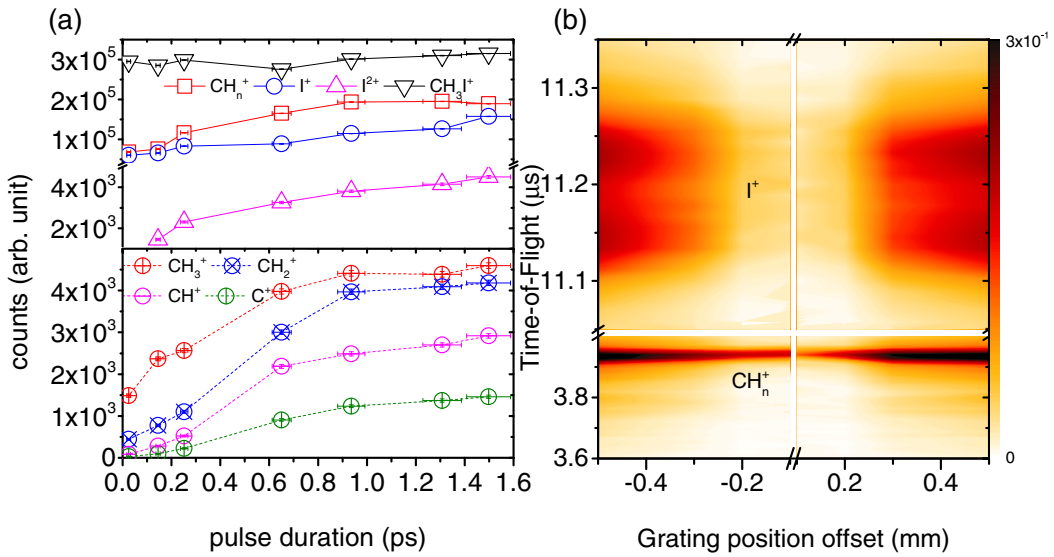

FIG. 2. (a) (Top) The measured absolute yields of the parent molecular ion CH_3I^+, CH_n^+, I^+, and I^{2+} ions, derived from the area under the corresponding peaks. (Bottom) The absolute yields of CH_n^+ ions coming in coincidence with I^+ (bottom) with the increasing pulse duration obtained by summing the counts in the islands in photoion-photoion coincidence. (b) A two-dimensional contour map of the ion time-of-flight spectrum (normalized with respect to the total counts) as a function of grating position offset. The offset is with respect to grating position for the shortest laser pulses. Negative offsets introduce negative chirps into the laser pulse and vice versa.

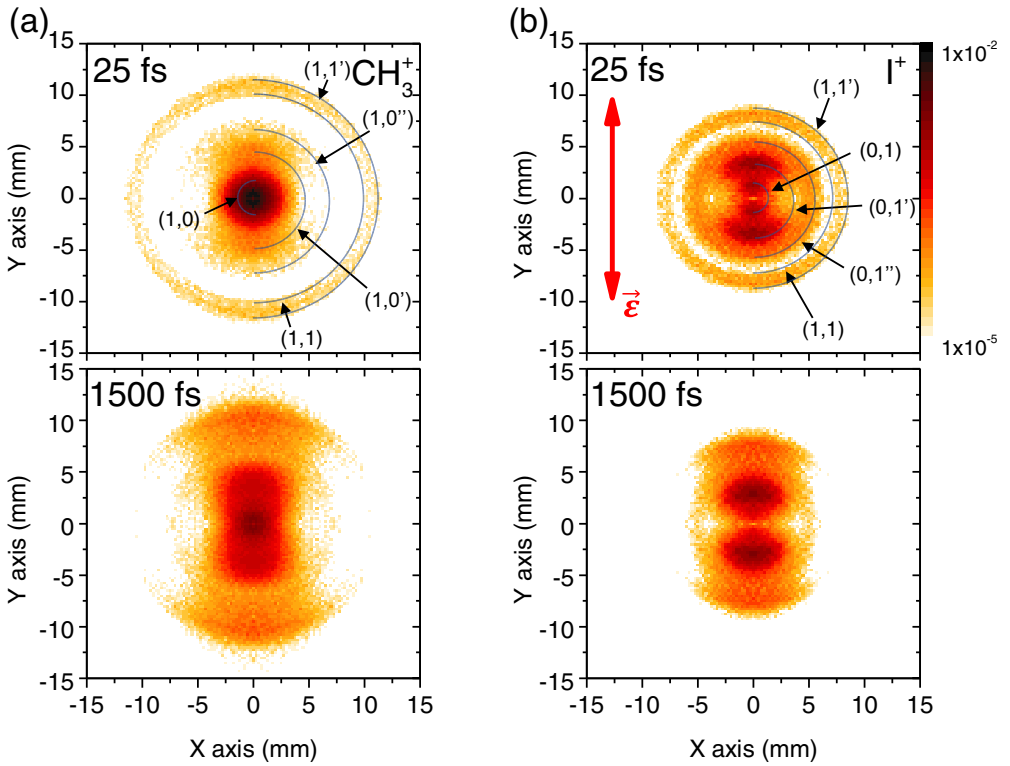

FIG. 3. Velocity map images of (a) CH_3^+ and (b) I^+ ions at shortest and longest pulse durations considered. The color scheme is in the logarithmic scale for the ion counts. The laser polarization axis (red arrow) is vertical. Semicircles identify different dissociation and CE channels. See text and Table I for more details.

intensity as before. In Fig. 3 we show the ion distribution map of the central velocity slice (ions ejected in the plane parallel to the detector and containing the laser polarization axis) of the two major ionic fragments CH_3^+ (left panel) and I^+ (right panel) at two pulse durations. The laser polarization axis is in the vertical direction in the figure. For the shortest pulse

TABLE I. The possible dissociation pathways with the peak kinetic energy (KE) obtained from the fitting and the corresponding kinetic energy release (KER), defined as the sum of energy of the fragments. The current data are compared with that of previous studies by Zhang *et al.* [11] and Liu *et al.* [12].

Fragmentation channel	Possible pathway	Kinetic energy (eV)	Kinetic energy release (eV)		
(p, q)		CH_3^+	$KE_{CH_3^+} \times m_{CH_3I}/m_{I^+}$		
			Our experiment	Zhang *et al.* [11]	Liu *et al.* [12]
(1, 0)	$CH_3I^+ (2E_{1/2}) \leftrightarrow CH_3I^+ (1E_{1/2} + 1\omega) \rightarrow CH_3^+ + I (^2P_{3/2})$	0.00	0.00		0–0.03
(1, 0′)	$CH_3I^+ (1E_{1/2}) \leftrightarrow CH_3I^+ (5E_{1/2} - 1\omega) \rightarrow CH_3^+ + I (^2P_{1/2})$	0.51	0.58		0.42
(1, 0″)	$CH_3I^+ (3E_{3/2}) \leftrightarrow CH_3I^+ (1E_{1/2} + 1\omega) \rightarrow CH_3^+ + I (^2P_{1/2})$	1.5	1.68		
(1, 1)	$CH_3I^{2+} \rightarrow CH_3^+ + I^+ (^3P_{1,0})$	2.9	3.2	3.6	3.1
(1, 1′)	$CH_3I^{2+} \rightarrow CH_3^+ + I^+ (^3P_2)$	3.5	4.0	4.1	4.0
(p, q)		I^+	$KE_{I^+} \times m_{CH_3I}/m_{CH_3^+}$		
			Our experiment	Zhang *et al.* [11]	Liu *et al.* [12]
(0, 1)	$CH_3I^+ (1E_{3/2}) \leftrightarrow CH_3I^+ (2E_{1/2} - 1\omega) \rightarrow CH_3 + I^+ (^3P_2)$	0.02	0.19		
(0, 1′)	$CH_3I^+ (2E_{1/2}) \rightarrow CH_3 + I^+ (^3P_2)$	0.07	0.65	0.56	0.66
(0, 1″)	$CH_3I^+ (3E_{3/2}) \rightarrow CH_3 + I^+ (^3P_2)$	0.18	1.70	1.40	
(1, 1)	$CH_3I^{2+} \rightarrow CH_3^+ + I^+ (^3P_{1,0})$	0.36	3.4	3.6	3.1
(1, 1′)	$CH_3I^{2+} \rightarrow CH_3^+ + I^+ (^3P_2)$	0.43	4.0	4.1	4.0

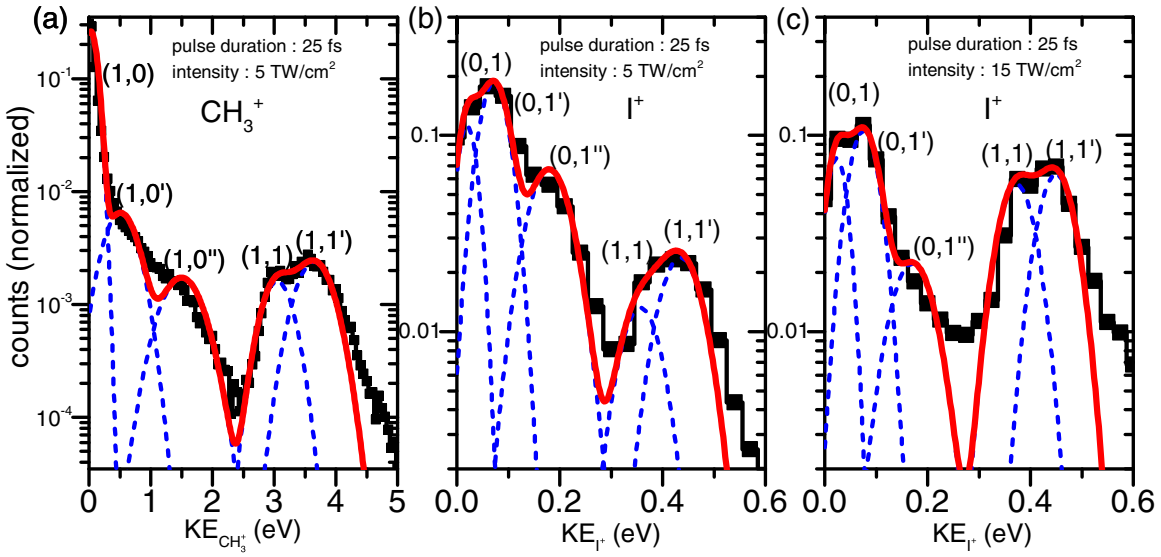

FIG. 4. The kinetic energy distribution (black histogram) of (a) CH_3^+ with multiple Gaussian fits (dashed blue and solid red curves) are shown for a peak intensity of ∼5 TW/cm^2 with pulse duration ∼25 fs. The same for I^+ ions at two different peak laser intensities. (b) ∼5 TW/cm^2 and (c) ∼15 TW/cm^2 with the same pulse duration.

duration, the map shows two distinct segments, with a nearly isotropic outer ring distribution for high-energy fragments and several dense distributions for the low-energy fragments near the center.

Figure 4 shows the kinetic energy (KE) distribution of the ionic fragments obtained by integrating the counts over the azimuthal angle at each radius. The KE distributions (with low-energy resolution) can also be obtained by inverting the ToF spectrum for the energetic fragments observed in the photoion-photoion coincidence map. A close correspondence (not shown here) of the latter KE distribution with that of the high-energy fragments in the velocity map images allow us to identify the outermost ring as arising from the Coulomb explosion (CE) of the doubly charged parent ion [23]. The low-energy ionic fragments are mainly due to the dissociation of the singly charged molecular ion into ionic and neutral fragments. All these breakup channels can be labeled in a (p, q) notation, where $p \geqslant 0$ denotes the charge states of $CH_3^{\,p+}$ ions and $q \geqslant 0$ does the same for I^{q+} ions. Multiple fragmentation channels with the same charge state are discriminated through a primed notation. We fit the KE distribution to a sum of Gaussian distributions corresponding to these (p, q) channels. Figure 4 shows the KE distribution of the CH_3^+ and I^+ ions at a pulse duration of ∼25 fs fitted with three Gaussian distributions for the low-energy fragments and two Gaussian distributions for the CE fragments. While the two CE peaks are quite evident for the CH_3^+ fragments, the low-energy resolution for I^+ hinders such a distinction. However, with higher intensity laser pulses [Fig. 4(c)], the CE channels are well populated and the two peaks are resolvable. It should be noted that even at these higher intensities, there is a relative variation in the yield of the channels, but no new channels are observed and, significantly, there is no shift in the peak positions for the CE channels either.

At the intensities used here, CH_3I^+ is populated largely in the spin-orbit split ground states $\widetilde{X}(1\ E_{3/2})$ and $\widetilde{X}(1\ E_{1/2})$ [15]. These states dissociate to give rise to CH_3^+ and the neutral I atom in the ground state. The higher excited state of $\widetilde{A}(2\ E_{1/2})$, which accounts for the near-zero energy I^+ ions, is also expected to be populated in the fast nonadiabatic ionization with the 25-fs laser pulses. To account for energetic fragments in dissociation, the involvement of higher excited states $\widetilde{B}(3\ E_{3/2}$ and $5\ E_{1/2})$ through a Floquet-type few-photon coupling can be reasonably postulated. Probable dissociation pathways correlating with energies obtained from the potential energy curves (PEC) [26] are listed in Table I. These are not unique assignments, especially for low-energy channels. For example, $CH_3I^+(1\ E_{3/2}) \leftrightarrow CH_3I^+(5\ E_{1/2}\text{-}2\omega) \rightarrow CH_3^+ + I(^2P_{1/2})$ can also produce CH_3^+ ions with ∼0.5 eV of energy, in addition to other channels leading to the same kinetic energy release. Here, the notation $(\langle \ldots \rangle \pm n\omega)$ indicates the dressing of the state with n laser photons. The bidirectional arrows indicate a coupling between the parent state and the dressed state. The molecule now dissociates along the modified coupled potential curve which exists only as long as the laser field [1,2,6,7]. In such a coupling, two modified potential curves arise resulting from the avoided crossing of the curves. On one of the curves, the molecule is stable against dissociation [2], known as bond hardening while the other curve aids dissociation (bond softening) [1]. The modified potential curves assigned for the dissociation channels here are those corresponding to bond softening. The two CE channels at ∼2.9 eV and ∼3.5 eV are assigned to the repulsive electronic states of the doubly charged parent ion leading to $CH_3^+ + I^+(^3P_{1,0})$ and $CH_3^+ + I^+(^3P_2)$, respectively, which matches well with previous studies [11,12].

As a function of pulse duration, the relative intensities of the dissociation channels change, but no new channels arise, and no shifts in their energies are seen. Significantly, however, we note that the CE channels $(1, 1)$ and $(1, 1')$ merge and shift towards the lower energies with increasing pulse duration. The KER of the CE channels progressively

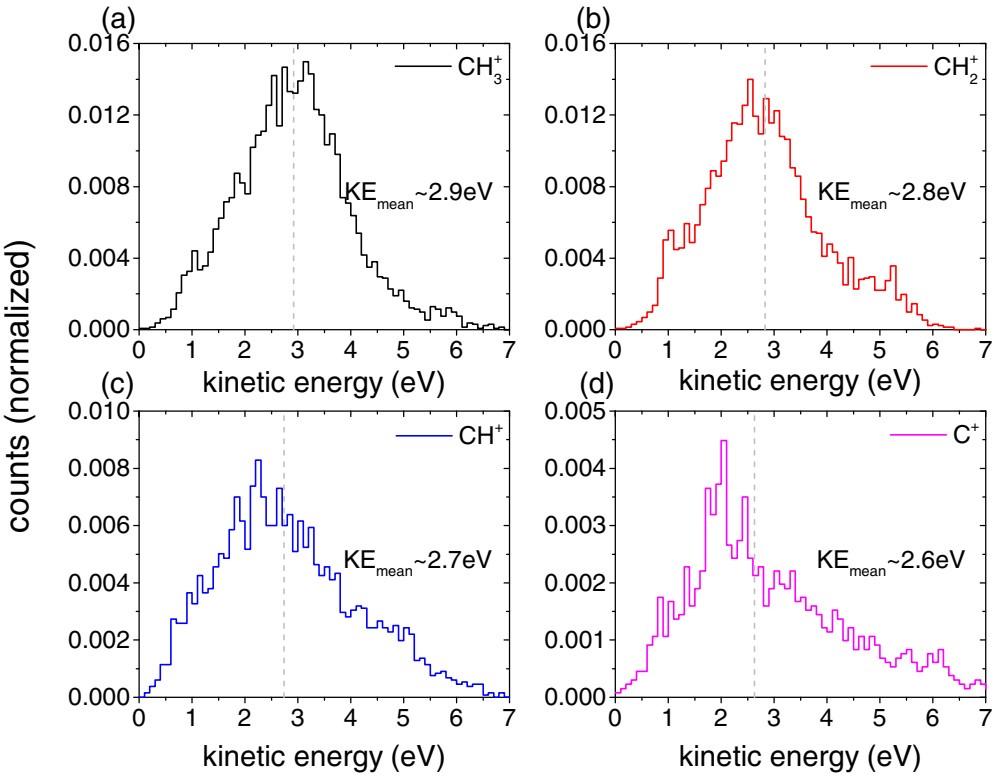

FIG. 5. The normalized KE distribution of the dehydrogenated ions (a) CH_3^+, (b) CH_2^+, (c) CH^+, (d) C^+ with respect to the total CH_n^+ counts coming in coincidence with the I^+ observed for the longest pulse duration in the photoion-photoion coincidence plot. The corresponding mean values of the distribution are highlighted in the plots with a dashed vertical line.

reduces from 3.6 and 4.1 eV (at 25 fs) to an unresolved broad peak at 3.2 eV (at 1500 fs). Furthermore, the nearly isotropic distribution becomes anisotropic as the pulse duration increases. The relative yield of these CE channels also increases with pulse duration, in line with the observations made in ToF mode. In the ToF mode, we also observe an enhancement in yields of dehydrogenated methyl fragments CH_m^+ ($m = 0$–2). The kinetic energy of these energetic ionic fragments coming in coincidence with I^+ ions can be estimated from the associated ToF spectrum. The kinetic energy distribution of these dehydrogenated methyl ionic fragments for the longest pulse duration (~1500 fs) has been shown in Fig. 5. The corresponding mean kinetic energies for these dehydrogenated methyl ionic fragments are ~2.9 eV of CH_3^+, ~2.8 eV of CH_2^+, ~2.7 eV of CH^+, and ~2.6 eV of C^+. This systematic trends associated with the kinetic energy of these dehydrogenated methyl ionic groups $KE_{CH_3^+} > KE_{CH_2^+} > KE_{CH^+} > KE_{C^+}$ remain unchanged with pulse duration variation. The mean kinetic energy of each of these fragments reduces by ~0.1 eV as compared to its precursor. We note here that the resolution of the spectrometer in the ToF mode is 0.08 eV [23] for these conditions. The relative kinetic energy difference between these dehydrogenated methyl ionic fragments is found to be independent of the pulse duration of the laser pulse. These observations suggest that these dehydrogenated ionic fragments arise from the CH_3^+ ions by stepwise dissociation. The stepwise dissociation of the parent CH_3^+ ion occurs just after the Coulomb explosion of the dicationic methyl iodide and the possible dissociation pathways are like [12]

(i) $CH_3^+ \rightarrow CH_2^+ + H$,
(ii) $CH_2^+ \rightarrow CH^+ + H$,
(iii) $CH^+ \rightarrow C^+ + H$.

In the above-mentioned dissociation processes, the neutral H atom is removed in each step and it carried away a small amount of energy which causes the shift in the kinetic energy of these dehydrogenated ionic fragments.

The ionic fragments I^{2+} arising from the dissociation of the dication or from the CE of the trication have also been collected in the imaging mode. Figure 6(a) shows the velocity distribution of the I^{2+} ions for ~150 fs pulse duration with the same peak intensity as before. The KE distribution of the I^{2+} ions shown in Fig. 6(b) is fitted with three Gaussian distributions, two for the low-energy fragments and one for the rest. The peak at ~0.2 eV can be associated with the asymmetric dissociation of CH_3I^{2+} ions through $(0, 2'')$ CH_3I^{2+} $(\tilde{X}\ ^2E_{1/2})$ $\rightarrow$ CH_3 + I^{2+} $(4\ ^0P_{3/2})$ channel. However, the origin of the other low-energy channel with a mean KE of ~0.1 eV is yet unknown. The high-energy peak (~0.8 eV) corresponds to a Coulomb explosion channel $(1, 2)$. This is confirmed by evaluating the KE of the fragments in the ToF spectrum filtered for ions in the $CH_n^+ + I^{2+}$ island. The assignment is also in agreement with previous studies [11]. Corrales *et al.* [10] assigned the same channel $CH_3I^{3+} \rightarrow CH_3^+ + I^{2+}$ $(^2P_{1/2})$ to a KE distribution peaking at ~1 eV. This higher KE (as compared to our observation and others [11]) has been attributed to the low pulse durations (50 fs) and higher intensities in their studies. In our experiments we failed to see any

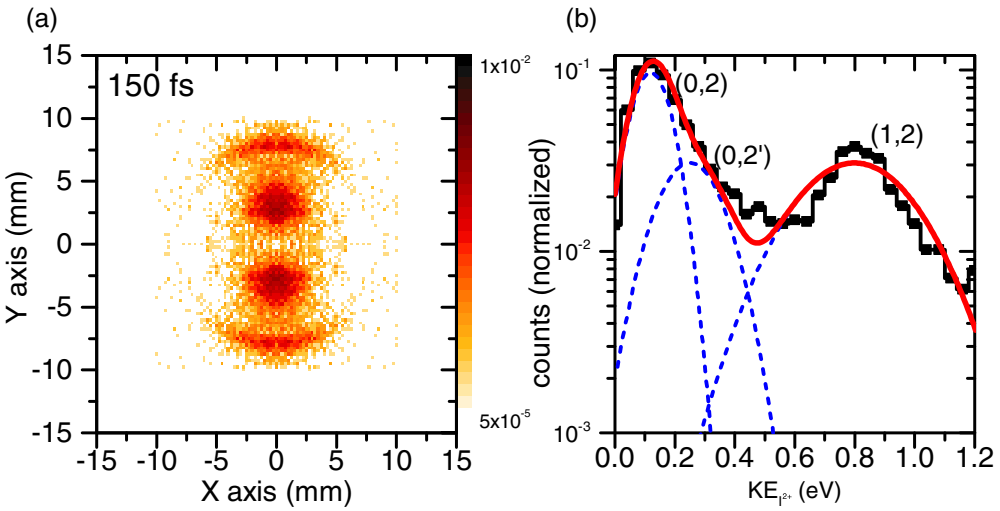

FIG. 6. (a) The velocity map Iiages of I^{2+} ions at pulse duration ∼150 fs with peak intensity ∼5 TW/cm^2 and the corresponding kinetic energy distribution (b) (black histogram) with multiple Gaussian fits are shown in dashed blue and solid red curves.

I^{2+} ions at ∼25 fs, indicating that a direct generation of CH_3I^{3+} at these intensities is not feasible. No significant change in the angular distribution with increased pulse duration is observed for the CE channel (1,2). However, the yield increases and the CE peak shifts towards lower energy (0.6 eV at 1500 fs).

IV. DISCUSSION

In the interaction of CH_3I with an ultrashort laser pulse of 25-fs duration in the moderate-intensity regime between 10^{12}–10^{13} W/cm^2, the ion is predominantly formed in the spin-orbit-coupled CH_3I^+ $\widetilde{X}$(1 $E_{3/2}$ and 1 $E_{1/2}$) states by removing a single electron from the outermost orbital (2*e*). This is a rapid, nonadiabatic Frank-Condon–type transition. The low-energy dissociation channels at the shortest laser pulse provide evidence that the low-lying excited states $\widetilde{A}$ (2 $E_{1/2}$) state and $\widetilde{B}$ states (3 $E_{3/2}$ and 5 $E_{1/2}$) are also populated through direct ionization. The rapid nonadiabatic ionization to any of these electronic states results in multiple rovibrational levels being excited by the laser pulse. A rovibrational wave packet evolving in time along the potential energy surface of the electronic state is initiated, mainly along the coordinate defined by the internuclear separation C-I. For the dication states too, direct ionization at the equilibrium geometry is predominant for short pulses. However, sequential ionization from the intermediate monocationic states should also be considered, particularly for longer laser pulses. It is therefore conceivable that the yield of the subsequent CE is also modulated by the evolving dynamics of the intermediate state. For example, in pump-probe studies, Malakar *et al.* [16] have observed through CEI, the C-I stretch vibrational mode (ν_3) in the $\widetilde{A}$ state of CH_3I^+. A consequence of this bond stretch in the molecule is an unequal shifting of the energies of molecular orbitals relative to each other. We propose that the variation in the yield and angular distributions as seen in the CE channels here reflects these dynamics.

Detailed multiconfiguration (MC) self-consistent (SCF) [27] based calculation in the field-free condition shows [see Fig. 7(a)] an energy uplift of the inner HOMO-1 (3*a*) orbital of the CH_3I^+ ion with increasing bond distance. The HOMO (2*e*) and HOMO-1 (3*a*) orbital merge near ∼4.5 Å. However, at r_c ∼ 3.9 Å the energy difference equals that of the laser photon energy, ∼1.5 eV, at which point the two orbitals could be efficiently coupled [9] in the presence of the laser field. Now, for example, let us consider the evolution of the intermediate state $\widetilde{A}$ following the ionization event of being populated at 2.14 Å. It takes about 70 fs for the C-I bond to stretch to 3.9 Å. For a 25-fs laser pulse, there is negligible laser intensity at this point. However, with longer laser pulses, the two orbitals could be resonantly coupled. In the coupled state, spatial localization of electrons can increase the ionization probability, depending on the geometrical overlap, the symmetry of the orbitals, and how they are oriented with respect to the laser polarization direction. With longer pulses, both the coupling and the subsequent ionization are effectively enhanced.

Multiorbital ionization also imposes stringent conditions on the angular distribution of the fragment ions. The observed angular distribution of these two channels at the shortest laser pulse of 25 fs shows a nearly isotropic distribution, which is expected if the main contribution for the ionized electron is the outermost HOMO (2*e*) orbital [18,19]. The velocity distributions in Fig. 3(a) of $CH_3{}^+$ for different pulse durations show the two CE channels broaden and shift towards the lower energy for pulses >650 fs and the angular distribution becomes increasingly anisotropic. It follows that the involvement of HOMO-1 (3*a*) orbital increases for larger pulse durations. The 3*a* orbital distributed close to the internuclear axis will be easily ionized if the laser polarization axis is parallel to the C-I bond and, hence, the large anisotropy in the observed CE ion distribution. From the angular distribution, we can attest that the dominant contribution at longer pulses to CE appears to be due to ionization from the $\widetilde{A}$ state, with the 3*a* orbital being increasingly involved at larger internuclear separations.

The (1,2) channel arises from the CE of the tricationic state of the methyl iodide. At these low-to-moderate intensities, a direct ionization to the tricationic state would be highly improbable. Sequential, enhanced ionization due to a stretch in

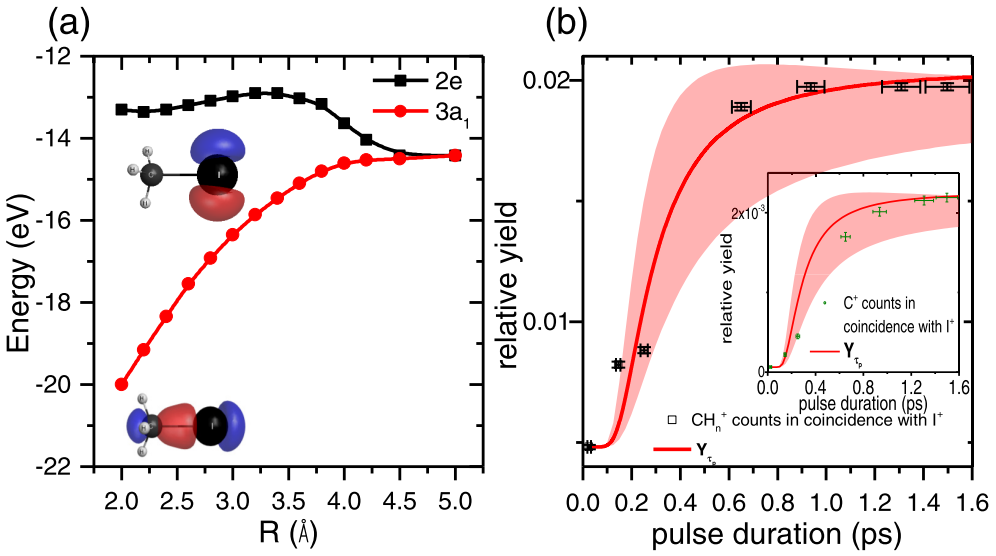

FIG. 7. (a) The energy of the HOMO $2e$ and HOMO-1 $3a_1$ orbitals of the monocationic methyl iodide obtained from MCSCF calculation. The electron distributions for the orbitals are shown within, indicating that the $3a_1$ electrons are distributed closer to the internuclear axis. The orbital energies are separated by 1.5 eV at 3.9 Å which suggests an enhanced probability of sequential ionization due to coupling of the two orbitals. (b) The relative yield of the coincident $CH_n^+ + I^+$ ions with respect to the total ion yield as a function of pulse duration. The calculated ionization probability as a function of pulse duration, based on a semiclassical model accounting for enhanced ionization due to a resonant coupling at an internuclear separation of ∼3.9 Å, is shown as a red solid line. The shaded region incorporates ionization probability assuming different single ionization times (within ±10% of the laser peak, see text). The enhancement of C^+ ions with increasing pulse duration has been shown in the inset with the corresponding model calculation.

the C-I bond is therefore a plausible explanation. We propose that a similar upshifting of orbital energy in the intermediate $\widetilde{A}$ enhances the ionization probability and is responsible for the formation of tricationic state. Figure 6 shows the I^{2+} ions arising from CE at a pulse duration of ∼150 fs with a broad energy distribution peaked at ∼0.82 eV and the angular distribution strongly peaked along the laser polarization axis. This anisotropic angular distribution suggests dominant HOMO-1 ($3a$) contribution to the ionization. However, the HOMO-1 contains only one electron in the $\widetilde{A}$ state configuration. It is possible that the second electron is contributed by the HOMO or HOMO-2 orbital, but the highly anisotropic angular distribution observed makes it unlikely. On the other hand, in the presence of the laser field, especially when the $2e$ and $3a$ orbitals are resonantly coupled ($r \rightarrow r_c$), interorbital electron transfer $3a \leftarrow 2e$ can occur [9,28]. So subsequently, both the electrons in the $3a$ orbital can be removed, more easily for molecular ions aligned parallel to the laser polarization axis, leading to the strongly anisotropic angular distribution.

The time evolution of the intermediate state can be visualized by a simple classical model by estimating bond stretching with time [17]. The molecular ion can be considered as a classical particle with the reduced mass "μ," moving over the PEC $V(r)$, defined by the C-I bond separation coordinate r. The dynamics of the particle can be tracked by solving the equation of motion $d^2r/dt^2 = -1/\mu \times dV(r)/dr$ over the electronic state. Assuming a Frank-Condon–type transition to the corresponding state from the ground state of the neutral CH_3I molecule at ionization, the C-I bond length is taken to be equilibrium bond length $r_e \sim 2.14$ Å at initiation $t = t_0$.

Here, we assume that the observed enhanced ionization signal is a consequence of the multiorbital resonance as proposed above. Then, the ionization probability of the cation in response to a single-cycle laser pulse [22] of wavelength 800 nm ($\hbar\omega = 1.55$ eV), at the bond length r can be considered to be of the form $P(r) \sim \exp[\frac{\Delta E(r)}{\Delta E(r)-\hbar\omega}]^2$, peaking around $r_c = 3.9$ Å. Here $\Delta E(r) = (E_{2e} - E_{3a_1})$ is the energy difference between the HOMO and HOMO-1 orbitals. The contribution to the multiple ionization signal for a multicycle laser pulse of duration τ_p would therefore be proportional to $Y_{\tau_p} = \int_{t_0}^{\infty}[I_{\tau_p}(t) \times P'(t)]\,dt$, $I_{\tau_p}(t)$ being the cycle-averaged envelope of the laser intensity. The ionization probability at any time t, $P'(t)$ is arrived at by computing the classical bond separation r at t using the PEC for the $\widetilde{A}$ state and thereby $P(r)$. For smaller values of τ_p, Y_{τ_p} would be small, as $I_{\tau_p}(t_c)$ is small at the peak of probability function r_c. With increasing τ_p, the integrated yield would increase rapidly as the field as $r = r_c$ increases. However, with fixed peak intensity, beyond a certain τ_p, the increase in yield will be incremental, as the increased laser field beyond $r = r_c$ has minimal contribution to Y_{τ_p}. Calculated values of Y_{τ_p} are shown in red in Fig. 7(b) and compared with the experimental yield of the energetic coincident ions for the $CH_n^+ + I^+$ islands. Here the experimental data are normalized to total counts in the ToF spectrum, while the Y_{τ_p} is scaled to match the extreme values of the normalized data. The solid red curve represents calculations considering the initiation of the wave-packet motion t_0, that is the single ionization event, occurs nominally at the peak of the laser pulse. The shaded band shows the variation in calculated yield where the ionization occurs within ±10% of the laser peak. The model calculations have also been compared with the total counts for CH_3^+ and I^+ ions [Fig. 2(a) (upper panel)] and the correspondence (not shown here) is poor. This is not surprising as the total counts also contain ions from the

dissociation from the single charged species. The dissociation also could be enhanced with many bond-softening pathways being accessed with longer pulses.

The dehydrogenated methyl ionic fragments also show similar enhancement with pulse duration increase as shown in Fig. 2(a) (bottom panel). As pointed out earlier, the kinetic energy distributions suggest stepwise dissociation from the parent $CH_3{}^+$ ions by releasing neutral H atoms at each dissociation step. The increasing anisotropy in the angular distribution of the precursor methyl ion points to the increasing involvement of the $3a$ orbital, aligned to the laser polarization axis, in the formation of the dicationic charge state of the CH_3I. The aligned molecule gets distorted from its tetrahedral structure due to the external electric field to that of the extreme turning point of an umbrella-mode vibration [29,30]. Such umbrella-mode vibration could initiate the stepwise dissociation and as the contribution of the prealigned molecules increases significantly in the Coulomb explosion with increasing pulse duration, so would the sequential dissociation of the dehydrogenated methyl ionic fragments. A close correspondence of the C^+ yield with the model calculations [inset of Fig. 7(b)] also supports our speculation. Nevertheless, the formation of atomic fragments at such low laser intensities in sub-ps laser pulses is significant and merits an involved analysis, which cannot be captured by the classical and phenomenological approach here. The possible role of intermediate electronic states also needs to be investigated. Quantum calculations, involving the rich dynamics of transient species [31] with interesting geometries, are essential to the understanding and out of the scope of this paper.

A discussion on the role of dispersion (chirp) in the laser pulse is pertinent here. We have noted that the yield of the fragmentation products and their mean energies both for dissociation and CE are be independent of the sign of the chirp. This is to be contrasted with experimental and theoretical results [32,33], wherein the role of chirp is distinguished by the difference in yields and changes in the mean energy of the products as a function of the sign of the chirp. For example, the central wavelength of the laser 800 nm, and a bandwidth of 50 nm corresponds to photons in the energy range of 1.55 $\pm$0.05 eV. For dissociation channels, with transitions induced by one photon, the change in the kinetic energy release with the dispersed wavelength will cause a change in KER by $\pm$0.05 eV. However, such a shift for the dissociation energies is not seen here, possibly hidden in the thermal energy spread ($\pm$0.025 eV) of the effusive molecular target. A significant shift ($\sim$1 eV) in the energies of the ions is only visible for the CE channels. The effective bandwidth due to multiphoton ($n = 15$) absorption to the dication states is $\pm$0.73 eV. Hence, only the ground, $2E + A_1$, and two excited states of CH_3I^{2+}, $E + A_2$ and A_1, are accessible within the bandwidth [10]. With increasing dispersion, no new upper electronic levels will be accessible, which could have accounted for a possible change in ionization probability. Furthermore, with a positively chirped laser pulse, high-frequency components arrive after the peak of the laser pulse. So, the dication and trications would form with higher excess energy than that due to the central wavelength photons. Consequently, with increasing positive chirp, the energy of the fragments would increase. Conversely, a negative chirp would see a drop in the fragment ion energy. Neither of these predictions is supported by our data, and we are justified in neglecting the role of dispersion for our interpretation.

The fair correspondence of the model calculations with the yield of the high-energy fragments needs to be qualified with some caveats. The classical model assumes ionization occurs near the peak of the laser pulse, within $\pm$10% of the laser peak. The assumption holds true for shorter pulses, but may not be valid for longer pulses. Experimentally, however, our observation is that, by keeping the peak intensity the same, the yield of the parent molecular ion CH_3I^+ does not change with increasing pulse duration. Furthermore, as is seen from the velocity map images, there are subtle changes in the yields of the various dissociation channels, but no new channels are observed, even with increased intensity. So, in this intensity range and in the NIR wavelength regime, it may be reasonable to assume that the low-lying bound electronic states populated nonadiabatically [20] at the shortest pulse duration, 25 fs, are the same as those observed for larger pulse duration.

The model, ascribing the ionization probability to a form as chosen above, is as of yet without a sound theoretical basis. A critical internuclear distance at, or beyond, which there is an enhanced ionization probability, has been shown for a number of molecules [3–5,8,9]. In associating the critical distance to a laser-induced orbital coupling at $r_c = 3.9$ Å we refer to other theoretical studies [22] to guess the form of the ionization probability. Conventionally, the experimental estimate of the critical distance is obtained by considering r_c as the distance of two point charges separated before the explosion and to equate the measured CE through $r_c(\text{Å}) = 14.4 \times (p \cdot q)/\text{KER(eV)}$. This yields a range of $r_c = 3.6$–4.2 Å from our measurements and from previous studies [11,12]. The choice of r_c therefore does not disagree with these observations. Nevertheless, it must be stated that a pump-probe experiment with carefully chosen intensities should be considered definitive to extract the critical distance.

We also point out that the model estimate for the yields at lower pulse durations deviates from the experimental results, which could be due to various reasons. Primarily, we have neglected the role of direct ionization, which is seen to have a nontrivial contribution for the $CH_n{}^+ + I^+$ yields, at low pulse durations. There could also be errors in the PEC due to the fixed geometry assumption taken for the methyl group [26], leading to erroneous calculations. The choice of the intermediate $\tilde{A}$ state is justified by considering previous studies [16] and keeping in mind the timescale of the dynamics. For example, in the repulsive state $\tilde{B}$ the time evolution of the wave packet is expectantly much faster, dissociating within $\sim$100 fs. In any case, the classical model serves only as an empirical guide to support our speculations and time-domain Schrödinger-equation solutions are essential to confirm the pathway assignment to the KER observed. Furthermore, if we strictly consider the symmetries of the orbitals involved, laser-induced dipole coupling between the orbitals parallel to the laser polarization direction is improbable. A time-domain density functional theory approach may hence be necessary to tackle the issue.

V. SUMMARY

CH_3I, interacting with moderate intensity laser pulses (5×10^{12} W/cm^2, 25–1500 fs) is mainly singly ionized with a significant fraction of these ions further dissociating in the laser field. But, even at these low-energy densities, dicationic and even tricationic states can be formed with longer duration laser pulses (>150 fs). Our investigations, through ion imaging of the fragments, aided with a simple classical 1D model suggest that a considerable contribution to this is through delayed sequential ionization in an intermediate state $\widetilde{A}$ in the monocation. With increased C-I bond separation, triggered at the formation of the ion, the inner $3a$ orbital upshifts in energy. If sufficient laser intensity exists, a resonant coupling is possible, even favoring pumping of the electron: $3a \leftarrow 2e$. Thus, longer laser pulses can further populate repulsive states of the CH_3I^{2+} and CH_3I^{3+} ions. A well-studied molecular system such as CH_3I is yet a source of rich and varied dynamical processes. Observations of some of these dynamics, reported here, need to be investigated in detail, both experimentally and theoretically in future work.

The data that support the findings of this study are available from the corresponding author upon reasonable request by email.

ACKNOWLEDGMENTS

V.S. and R.G. thank Professor M. Krishnamurthy for the usage of the laser facilities and Dr. R. Ramakrishnan for extending to us the computational facilities of the Tata Institute of Fundamental Research, Hyderabad, and for insightful suggestions. The funding from DST-SERB, DAE-BRNS, IMPRINT, UKIERI, and SPARC is gratefully acknowledged.

[1] P. H. Bucksbaum, A. Zavriyev, H. G. Muller, and D. W. Schumacher, Softening of the H_2^+ Molecular Bond in Intense Laser Fields, Phys. Rev. Lett. **64**, 1883 (1990).

[2] L. J. Frasinski, J. H. Posthumus, J. Plumridge, K. Codling, P. F. Taday, and A. J. Langley, Manipulation of Bond Hardening in H_2^+ by Chirping of Intense Femtosecond Laser Pulses, Phys. Rev. Lett. **83**, 3625 (1999).

[3] D. Pavičić, A. Kiess, T. W. Hänsch, and H. Figger, Intense-Laser-Field Ionization of the Hydrogen Molecular Ions H_2^+ and D_2^+ at Critical Internuclear Distances, Phys. Rev. Lett. **94**, 163002 (2005).

[4] T. Zuo and A. D. Bandrauk, Charge-resonance-enhanced ionization of diatomic molecular ions by intense lasers, Phys. Rev. A **52**, R2511(R) (1995).

[5] A. D. Bandrauk and J. Ruel, Charge-resonance-enhanced ionization of molecular ions in intense laser pulses: Geometric and orientation effects, Phys. Rev. A **59**, 2153 (1999).

[6] A. Hishikawa, S. Liu, A. Iwasaki, and K. Yamanouchi, Light-induced multiple electronic-state coupling of O_2^+ in intense laser fields, J. Chem. Phys. **114**, 9856 (2001).

[7] A. Sen, T. Sairam, S. R. Sahu, B. Bapat, R. Gopal, and V. Sharma, Hindered alignment in ultrashort, intense laser-induced fragmentation of O_2, J. Chem. Phys **152**, 014302 (2020).

[8] I. Bocharova, R. Karimi, E. F. Penka, J.-P. Brichta, P. Lassonde, X. Fu, J.-C. Kieffer, A. D. Bandrauk, I. Litvinyuk, J. Sanderson, and F. Légaré, Charge Resonance Enhanced Ionization of CO_2 Probed by Laser Coulomb Explosion Imaging, Phys. Rev. Lett. **107**, 063201 (2011).

[9] S. Erattupuzha, C. L. Covington, A. Russakoff, E. Lötstedt, S. Larimian, V. Hanus, S. Bubin, M. Koch, S. Gräfe, A. Baltuška, X. Xie, K. Yamanouchi, K. Varga, and M. Kitzler, Enhanced ionisation of polyatomic molecules in intense laser pulses is due to energy upshift and field coupling of multiple orbitals, J. Phys. B: At. Mol. Opt. Phys. **50**, 125601 (2017).

[10] M. E. Corrales, G. Gitzinger, J. González-Vázquez, V. Loriot, R. de Nalda, and L. Bañares, Velocity map imaging and theoretical study of the coulomb explosion of CH_3I under intense femtosecond IR pulses, J. Chem. Phys. A **116**, 2669 (2012).

[11] D. Zhang, S. Luo, H. Xu M. Jin, F. Liu, B. Yan, Z. Wang, H. Liu, D. Jiang, A. Eppink, W. Roeterdink, S. Stolte, and D. Ding, Dissociative ionization and Coulomb explosion of CH_3I in intense femtosecond laser fields, Eur. Phys. J. D **71**, 148 (2017).

[12] H. Liu, Z. Yang, Z. Gao, and Z. Tang, Ionization and dissociation of CH_3I in intense laser field, J. Chem. Phys. **126**, 044316 (2007).

[13] Y. Wang, S. Zhang, Z. Wei, and B. Zhang, Velocity map imaging of dissociative ionization and coulomb explosion of CH_3I induced by a femtosecond laser, J. Phys. Chem. A **112**, 3846 (2008).

[14] S. Marggi Poullain, D. V. Chicharro, J. González-Vázquez, L. Rubio-Lago, and L. Bañares, A velocity map imaging study of the photodissociation of the methyl iodide cation, Phys. Chem. Chem. Phys. **19**, 7886 (2017).

[15] Z. Wei, J. Li, S. T. See, and Z.-H. Loh, Spin–orbit state-selective C-I dissociation dynamics of the CH_3I^+X electronic state induced by intense few-cycle laser fields, J. Phys. Chem. Lett. **8**, 6067 (2017).

[16] Y. Malakar, W. L. Pearson, M. Zohrabi, B. Kaderiya, P. Kanaka, Raju F. Ziaee, S. Xue, A. T. Le, I. Ben-Itzhak, D. Rolles, and A. Rudenko, Time-resolved imaging of bound and dissociating nuclear wave packets in strong-field ionized iodomethane, Phys. Chem. Chem. Phys. **21**, 14090 (2019).

[17] M. E. Corrales, J. González-Vázquez, R. de Nalda, and L. Bañares, Coulomb explosion imaging for the visualization of a conical intersection, J. Phys. Chem. Lett. **10**, 138 (2019).

[18] A. H. Alexander, G. Basnayake, D. A. Debrah, Y. F. Lin, S. K. Lee, P. Hoerner, Q. Liao, H. Schlegel, and W. Li, Disentangling strong-field multielectron dynamics with angular streaking, J. Phys. Chem. Lett **9**, 2539 (2018).

[19] S. G. Walt, N. Bhargava Ram, A. von Conta, O. I. Tolstikhin, L. B. Madsen, F. Jensen, and H. J. Wörner, Role of multielectron effects in the asymmetry of strong-field ionization and fragmentation of polar molecules: The methyl halide series, J. Phys. Chem. A **119**, 11772 (2015).

[20] S. Das, P. Sharma, and R. K. Vatsa, Tracing photoionisation behavior of methyl iodide in gas phase: From isolated molecule to molecular aggregate, J. Photochem. Photobiol. C **33**, 27 (2017).

[21] K. Harumiya, H. Kono, Y. Fujimura, I. Kawata, and A. D. Bandrauk, Intense laser-field ionization of H_2 enhanced by two-electron dynamics, Phys. Rev. A **66**, 043403 (2002).

[22] S. Chattopadhyay and L. B. Madsen, Electron correlation effects in enhanced ionization of diatomic molecules in near-infrared fields, Phys. Rev. A **99**, 023424 (2019).

[23] R. Gopal, A. Sen, S. R. Sahu, A. S. Venkatachalam, M. Anand, and V. Sharma, Note: An ion imaging spectrometer for studying photo-induced fragmentation in small molecules, Rev. Sci. Instrum. **89**, 086107 (2018).

[24] B. Alonso, Í. J. Sola, and H. Crespo, Self-calibrating d-scan: Measuring ultrashort laser pulses on-target using an arbitrary pulse compressor, Sci. Rep. **8**, 3264 (2018).

[25] A Rudenko, K. Zrost, C. D. Schröter, V. L. B. de Jesus, B. Feuerstein, R. Moshammer, and J. Ullrich, Resonant structures in the low-energy electron continuum for single ionization of atoms in the tunneling regime, J. Phys. B: At. Mol. Opt. Phys. **37**, L407 (2004).

[26] M. Tadjeddine, J. P. Flament, and C. Teichteil, Spin-orbit calculations of the molecular states of CH_3I^+, related to photofragmentation experiments, Chem. Phys. **124**, 13 (1988).

[27] P. G. Szalay, T. Müller, G. Gidofalvi, H. Lischka, and R. Shepard, Multiconfiguration self-consistent field and multireference configuration interaction methods and applications, Chem. Rev. **112**, 108 (2012).

[28] G. L. Kamta and A. D. Bandrauk, Nonsymmetric molecules driven by intense few-cycle laser pulses: Phase and orientation dependence of enhanced ionization, Phys. Rev. A **76**, 053409 (2007).

[29] P. Graham, K. W. D. Ledingham, R. P. Singhai, M. Hankin, T. McCanny, X. Fang, C. Kosmidis, P. Tzallas, P. F. Taday, and A. J. Langley, On the fragment ion angular distributions arising from the tetrahedral molecule CH_3I, J. Phys. B: At. Mol. Opt. Phys. **34**, 4015 (2001).

[30] A. T. J. B. Eppink and D. H. Parker, Energy partitioning following photodissociation of methyl iodide in the A band: A velocity mapping study, J. Chem. Phys **110**, 832 (1999).

[31] B. Jochim, R. Siemering, M. Zohrabi, O. Voznyuk, J. B. Mahowald, D. G. Schmitz, K. J. Betsch, Ben Berry, T. Severt, N. G. Kling, T. G. Burwitz, K. D. Carnes, M. F. Kling, I. Ben-Itzhak, E. Wells, and R. de Vivie-Riedle, The importance of Rydberg orbitals in dissociative ionization of small hydrocarbon molecules in intense laser fields, Sci. Rep. **7**, 4441 (2017).

[32] J. Cao, C. J. Bardeen, and K. R. Wilson, Molecular Π pulses: Population inversion with positively chirped short pulses, J. Chem. Phys. **113**, 1898 (2000).

[33] J. Plenge, A. Wirsing, C. Raschpichler, M. Meyer, and E. Rühl, Chirped pulse multiphoton ionization of nitrogen: Control of selective rotational excitation in $N_2^+(B^2\Sigma_u^+)$, J. Chem. Phys. **130**, 244313 (2009).